

What Positional Embeddings Really Do In Vision Transformers

Anonymous Authors¹

Abstract

Positional embeddings (PEs) in Vision Transformers (ViTs) are typically viewed as mechanisms for injecting absolute spatial information. We show that ViTs trained without PEs can nonetheless recover non-trivial spatial structure using patch content alone, questioning the fundamental functional role of PEs. We demonstrate that PEs induce a sharp increase in early-layer representational diversity, characterized by higher effective rank and reduced token homogenization. However, our analysis reveals that this diversity alone is insufficient for robustness. Using a new metric, Spatial Similarity Distance Correlation (SSDC), we show that PEs facilitate a qualitative shift from content-based to absolute-position-based spatial organization, yielding representations that remain stable under distributional shifts where content-only models fail.

1. Introduction

Vision Transformers (ViTs) have emerged as a powerful alternative to convolutional architectures for visual recognition by modeling images as sequences of patch tokens processed through self-attention mechanisms (Dosovitskiy et al., 2021). Unlike Convolutional Neural Networks (CNNs), ViTs lack strong built-in biases toward locality and translation equivariance. To compensate, most ViT architectures rely on Positional Embeddings (PEs) to inject explicit spatial information, allowing the model to distinguish patches originating from different locations in the image.

Existing studies suggest that ViTs can retain substantial performance even when positional information is removed or degraded (Chu et al., 2023). This potentially indicates that transformers partially reconstruct spatial relationships from patch content alone, analogous to how CNNs learn

implicit positional information from zero-padding (Islam* et al., 2020). These findings challenge the conventional view that PEs are strictly necessary and raise fundamental questions about what functional advantages they provide beyond basic spatial identifiability.

Prior work has largely explored positional embeddings through downstream performance or architectural variations. While informative, such approaches reveal little about how PEs shape the internal representations of the model. In particular, the effects of positional embeddings on the geometry, dimensionality, and stability of token representations across the transformer stack remain poorly understood.

In this work, we adopt a mechanistic perspective to study the role of positional embeddings in ViTs. We analyze the evolution of token representations in the residual stream using tools from representational geometry (Raghu et al., 2021), introducing the Spatial Similarity Distance Correlation (SSDC), a metric designed to quantify how spatial relationships are reflected in token similarity patterns. Using this framework, we systematically compare ViTs trained with and without positional embeddings, examining their impact on representational dimensionality, the spatial reasoning strategies employed by the model, and robustness to distributional shifts such as stylization and noise. Using this framework, we demonstrate that PEs perform three critical functions:

- **Promoting Representational Diversity:** PEs causally increase representational diversity (characterized by high dimensionality and lower token similarities), thereby enriching internal geometric representations.
- **Shifting Spatial Organization Strategy:** We demonstrate that PEs push ViTs from a dominantly content-based strategy of forming internal spatial structure to an absolute-position-based strategy, where the model can always reason "where" a patch is without a great dependence on what it "looks" like.
- **Enhancing Robustness to Distributional Shifts:** We show that this absolute-position-based shift is precisely what allows ViTs with PEs to remain robust to distributional shifts, such as stylization, where local patch content becomes unreliable.

¹Anonymous Institution, Anonymous City, Anonymous Region, Anonymous Country. Correspondence to: Anonymous Author <anon.email@domain.com>.

Preliminary work. Under review by the International Conference on Machine Learning (ICML). Do not distribute.

055 Together, our results provide a detailed and novel view of
 056 how explicit positional signals shape the internal organization
 057 of vision transformers, offering new insights into
 058 why positional embeddings play a critical role in stable and
 059 robust visual representation learning.
 060

061 2. Background and Setup

062 2.1. Vision Transformer Architecture

063 All models used in our experiments are vanilla Vision Trans-
 064 formers trained from scratch, with approximately 12M pa-
 065 rameters. Images are divided into fixed-size patches, which
 066 are linearly projected into token embeddings and processed
 067 by a stack of self-attention and feedforward layers. When
 068 present, positional embeddings are learned parameters opti-
 069 mized jointly with the rest of the model. No architectural
 070 modifications or auxiliary inductive biases are introduced
 071 beyond standard ViT components.
 072

073 2.2. Positional Embedding Ablation

074 To isolate the functional role of positional embeddings, we
 075 train a parallel set of models in which positional embed-
 076 dings are entirely removed. Throughout the paper, we refer
 077 to models trained without positional embeddings as *ablated*
 078 *models*, and to models trained with positional embeddings
 079 as *intact models*. Apart from the presence or absence of po-
 080 sitional embeddings, all architectural choices, optimization
 081 settings, and training procedures are held constant.
 082

083 2.3. Datasets

084 We evaluate models on CIFAR-10 and a stylized variant
 085 derived from CIFAR-10 to assess robustness under distribu-
 086 tional shift. The stylized dataset is generated using Adaptive
 087 Instance Normalization (AdaIN) with a mixing coefficient
 088 $\alpha = 0.1$, which significantly alters texture statistics while
 089 preserving coarse spatial structure. Models are trained on
 090 standard CIFAR-10 images and evaluated on both the origi-
 091 nal and stylized datasets.
 092

093 3. Methods

094 3.1. Residual Stream Geometry

095 To analyze the evolution of internal representations across
 096 depth, we extract the residual stream at selected layers of
 097 the model (layers 0, 2, 4, and 9, where layer 9 corresponds
 098 to the final layer). At each layer, we represent the residual
 099 stream as a matrix $R \in \mathbb{R}^{T \times C}$, where T denotes the number
 100 of tokens and C the embedding dimension. Each row of R
 101 corresponds to the residual stream representation of a single
 102 token.
 103

104 Given the singular values $\{\sigma_i\}$ of R , we compute the effec-
 105

106 tive rank using the participation ratio:

$$ER = \frac{(\sum_i \sigma_i^2)^2}{\sum_i \sigma_i^4}.$$

107 Effective rank quantifies the number of dimensions that
 108 meaningfully contribute to the representation, with higher
 109 values indicating more distributed and heterogeneous repre-
 110 sentations.
 111

In addition, we compute pairwise cosine similarities be-
 112 tween all token representations in R to form a token cosine
 113 similarity matrix, where the (i, j) -th entry corresponds to
 114 the cosine similarity between tokens i and j . This matrix
 115 is symmetric by construction. We average the token cosine
 116 similarity matrix across the batch dimension to obtain a
 117 layer-wise summary of inter-token relationships. This ma-
 118 trix serves both as a proxy for inter-token heterogeneity and
 119 as the basis for computing the Spatial Similarity Distance
 120 Correlation (SSDC).
 121

122 3.2. Spatial Similarity Distance Correlation

To quantify the emergence of spatial structure, we introduce
 123 the Spatial Similarity Distance Correlation (SSDC). For a
 124 given layer, we compute the pairwise cosine similarity ma-
 125 trix between token representations and the corresponding
 126 matrix of pairwise spatial distances between token positions,
 127 where Spatial distance is defined as the Manhattan distance
 128 between patch coordinates on the image grid. SSDC is
 129 defined as the Spearman rank correlation between cosine
 130 similarity and the negative spatial distance, such that higher
 131 values indicate that tokens which are spatially closer tend to
 132 have more similar representations. Because SSDC measures
 133 the monotonic alignment between spatial proximity and rep-
 134 resentational similarity, it serves as a proxy for the presence
 135 of relative positional structure in the residual stream. We
 136 use Spearman rank correlation to remain agnostic to the
 137 precise functional form relating spatial distance and rep-
 138 resentational similarity.
 139

140 3.3. Fragility Score

To quantify a model’s sensitivity to distributional shifts, we
 141 define a simple *Fragility Score* (FS), which measures the
 142 relative drop in top-1 accuracy under distribution shift. It is
 143 defined as

$$FS = 1 - \frac{A_{shift}}{A_{normal}},$$

144 where A_{normal} and A_{shift} denote top-1 accuracy on the normal
 145 and shifted datasets, respectively. Higher values indicate
 146 greater performance degradation.
 147

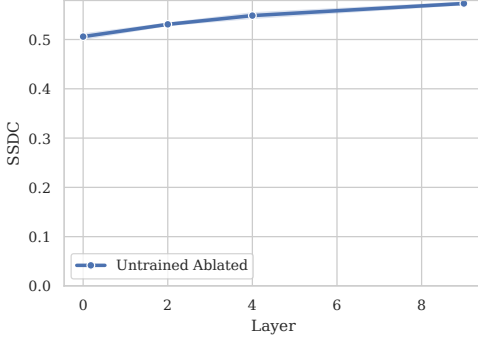


Figure 1. SSDC across depth for an untrained ablated model. SSDC remains approximately constant and at a relatively high value across layers, indicating static spatial correlations induced by architectural and data priors rather than learning. Shaded regions indicate variability across runs (± 1 standard deviation).

4. Results

4.1. Architectural Priors Induce Static Spatial Correlations at Initialization

Experimental Setup: We evaluate SSDC at layers 0, 2, 4, and 9 on the CIFAR-10 dataset using untrained ablated models. We also extract from each one of these layers the Token Cosine Similarity Matrix and plot them using the same color scale.

Results: The untrained ablated model exhibits a non-zero SSDC (0.5) that remains approximately constant across depth (Fig. 1). This behavior is consistent across runs and indicates the presence of static spatial correlations induced by architectural and data priors rather than learning. Importantly, SSDC magnitude alone is insufficient to characterize learned spatial organization; instead, changes in SSDC across depth are the relevant signal.

This static spatial structure can be visually demonstrated by token cosine similarity heatmaps that are shown in Appendix Fig. A1.

This provides a static baseline against which we can measure the emergence of learned spatial structure in trained models.

4.2. Validating Emergent Spatial Structure via Extreme Counterfactuals

Experimental setup: We compute Token Cosine Similarity Matrices from layers 0, 2, 4, and 9 and evaluate the SSDC on each of these layers. We compare three settings: (i) an untrained ablated model with tokens randomly permuted at inference time, serving as an extreme baseline with no spatial structure; (ii) a trained model without positional embeddings (trained ablated); and (iii) a fully trained intact model.

Results: The untrained ablated model with random permutation consistently exhibits a near-zero and depth-invariant

SSDC value, reflecting the absence of meaningful spatial organization in token representations. In contrast, the trained ablated model shows a clear and consistent increase in SSDC from layer 0 to layer 2, after which SSDC remains roughly constant across deeper layers (Fig. 3). This depth-dependent increase indicates the emergence of non-trivial spatial structure during training, despite the absence of explicit positional embeddings.

As expected, the trained intact model exhibits higher SSDC values across all layers, consistent with the direct contribution of explicit positional embeddings. Importantly, however, the presence of a strong SSDC increase in the trained ablated model demonstrates that spatial structure is not solely inherited from positional embeddings, but can emerge implicitly through training dynamics and architectural biases.

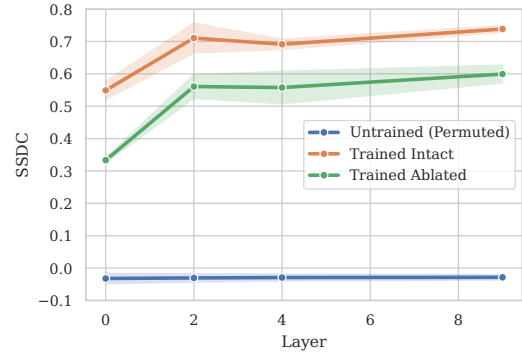


Figure 2. SSDC across depth for an untrained ablated model with random permutation, a trained ablated model, and a trained intact model. Shaded regions indicate variability across runs (± 1 standard deviation).

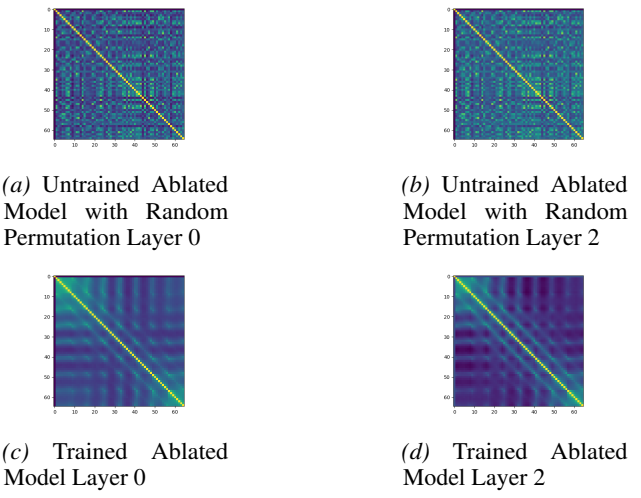
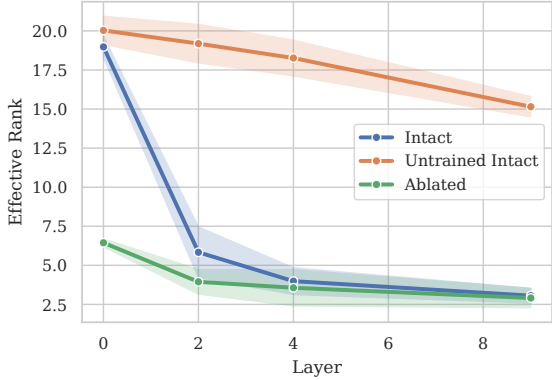
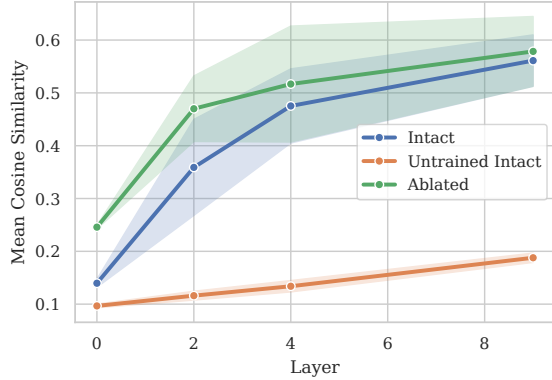


Figure 3. Representative token cosine similarity matrices. All matrices share the same color scale.



(a) Effective Rank across depth (Intact vs Post-hoc Ablated vs Untrained Intact).



(b) Mean Token Cosine Similarity across depth (Intact vs Post-hoc Ablated vs Untrained Intact).

Figure 4. Early-layer representational diversity under intact and post-hoc ablated positional embeddings. Left: Effective Rank of the residual stream across layers. Right: Mean token-wise cosine similarity across layers. Results are shown for a fully intact ViT, the same trained model with positional embeddings removed post-hoc at inference time, and a completely untrained intact model. The intact model exhibits substantially higher Effective Rank at layer 0 followed by an early collapse, while the post-hoc ablated model starts from a low-rank regime and remains consistently lower. Mean token cosine similarity is higher for the post-hoc ablated model across all layers.

4.3. Positional Embeddings Inject Early-Layer Representational Diversity

Experimental setup: We evaluate representational diversity in Vision Transformers using two complementary metrics: the Effective Rank of the residual stream and the mean token-wise cosine similarity. Experiments are conducted on CIFAR-10 using two models: (1) a standard ViT with intact positional embeddings, (2) the same trained model with positional embeddings removed post-hoc at inference time, and (3) an untrained model with untrained PEs initialized at random.

Effective Rank is computed at layers 0, 2, 4, and 9, following standard practice as a proxy for the dimensional diversity of representations. In parallel, we compute the token-to-token cosine similarity matrix at the same layers and report its mean value as a measure of representational collapse across spatial tokens.

Crucially, because positional embeddings are removed only at inference time, any observed differences reflect the functional role of positional information during forward computation rather than differences in learned parameters. Additionally, by observing the behavior of the untrained intact model, we can distinguish functionally meaningful representational diversity from representational diversity that is a result of random noise injections.

Results: Figure 4 reveals a pronounced difference in representational diversity between intact and post-hoc ablated models that emerges immediately at the input layer. At layer 0, the intact model exhibits an Effective Rank approximately four times higher than that of the post-hoc ablated model, indicating that positional embeddings inject substantial high-

dimensional diversity directly into the residual stream prior to any attention-based mixing.

Strikingly, this initial advantage does not persist unaltered. The intact model undergoes a sharp collapse in Effective Rank within the first two layers, after which its rank stabilizes and remains only slightly higher than that of the post-hoc ablated model for the remainder of the network. In contrast, the post-hoc ablated model begins in a low-rank regime and does not exhibit a comparable early collapse, instead maintaining a relatively stable but consistently lower Effective Rank across depth.

Mean token cosine similarity provides a complementary perspective. Across all layers and all runs, the post-hoc ablated model exhibits significantly higher token-wise similarity than the intact model, indicating persistent spatial homogenization when positional embeddings are removed. This elevated similarity is present from the earliest layer and does not disappear with depth, suggesting that the lack of positional information induces a sustained form of representational collapse across tokens.

Comparing the evolution of representational diversity across depth, we observe that untrained intact models do not exhibit the sharp post-early-layer collapse in effective rank seen in trained intact models. Consistent with this, the mean token-wise cosine similarity in untrained intact models remains approximately constant across depth, in contrast to the progressive increase observed in trained models.

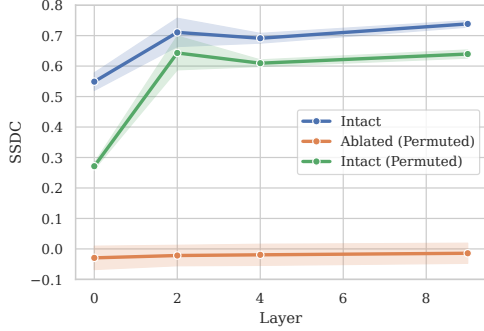


Figure 5. SSDC across depth for intact models, and intact/ablated models that have had their tokens permuted randomly at inference. The SSDC collapses to near-zero values upon permutation of the tokens of the ablated model, whereas the intact model’s SSDC only takes a slight hit after permutation. Shaded regions indicate variability across runs (± 1 standard deviation).

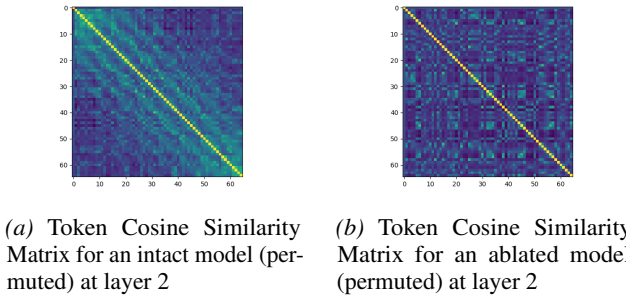


Figure 6. Representative Token Cosine Similarity Matrices. Once its tokens are permuted, the ablated model’s Token Cosine Similarity Matrix becomes chaotic and loses all spatial structure, whereas the diagonal band persists (though fuzzier) in the intact model’s.

4.4. Patch-Relative and Absolute-Position-Based Modes of Spatial Organization

Experimental Setup: We extract Token Cosine Similarity Matrices from layers 0, 2, 4, and 9 from intact models, permuted intact models, and permuted ablated models. We plot these matrices and evaluate the SSDC across depth.

Notably, this permutation allows us to probe whether spatial organization is anchored to absolute position or emerges purely from patch content. Since token cosine similarity matrices are constructed according to token indices, this permutation disrupts the correspondence between matrix proximity and spatial proximity. Consequently, any diagonal structure observed after permutation cannot be attributed to local patch relationships and instead reflects the model’s reliance on absolute positional information.

Results: We find that ablated models collapse to near-zero SSDC values after permutation (Fig. 5). Combined with the fact that these models’ performance remains unchanged un-

der permutation (Appendix Fig. A2), this indicates that ablated models form spatial structure primarily through patch content and relative relationships, without reliance on absolute token indices. As a result, permuting token order has no effect on which tokens become more similar as representations propagate through the network.

In contrast, intact models exhibit only a modest reduction in SSDC under permutation, suggesting that they rely more strongly on absolute token indices to organize spatial structure.

Interestingly, the SSDC of intact models under permutation drops sharply at layer 0 before gradually recovering across subsequent layers, remaining slightly below the unpermuted intact baseline. This pattern suggests that absolute positional information introduced by positional embeddings is progressively integrated within the encoder blocks, rather than being fully expressed at the input layer.

These trends are visually corroborated by the Token Cosine Similarity Matrices (Fig. 6). In the ablated models, permutation leads to a complete collapse of spatial structure, yielding matrices that appear random and unstructured. In contrast, intact models retain a fuzzy diagonal pattern after permutation, potentially suggesting that even intact models may partially rely on patch-content for spatial structure.

4.5. Robustness Is Tightly Linked to Spatial Encoding Strategy

Experimental Setup: We evaluate Fragility Scores as defined in section 3.3 across three distinct training and inference regimes designed to disentangle patch-content-based spatial organization from absolute-position-based strategies. The first regime is an intact model, trained and evaluated under standard conditions with positional embeddings (PEs) enabled. The second is an ablated model, in which positional embeddings are removed during and after training, serving as a reference point for models that lack explicit access to absolute position information. The third regime is an intact model trained with Random Permutation Training and evaluated with Random Permutation at Inference, hereafter referred to as RPT-RPI Intact.

The RPT-RPI Intact model preserves positional embeddings throughout training and inference, but is exposed to a different random permutation of patch tokens at every forward pass. As a result, any fixed mapping between token index and spatial location is systematically destroyed. This prevents the model from exploiting absolute positional cues, even though PEs are present in the architecture. Importantly, this regime does not collapse representational diversity: prior analyses show that RPT-RPI Intact models retain a large fraction of the effective rank and avoid the degeneracies observed in fully ablated models, although diversity

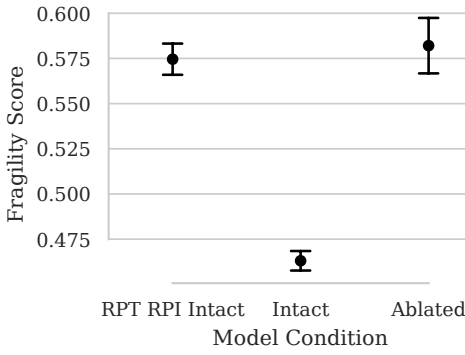


Figure 7. Fragility scores for intact, ablated, and permutation-trained intact models under the stylized dataset. Black markers show the mean Fragility Scores with ± 1 standard deviation. Intact models are substantially more robust, while permutation-trained intact models exhibit fragility comparable to ablated models despite retaining positional embeddings.

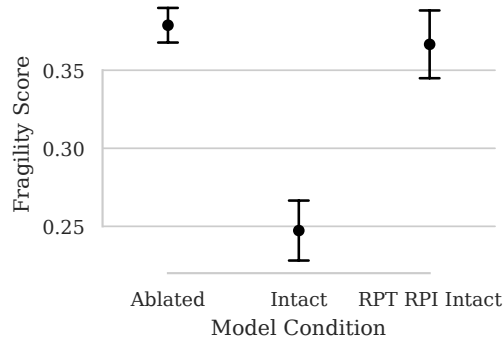


Figure 8. Fragility scores for intact, ablated, and permutation-trained intact models exposed to Gaussian Blur. Black markers show the mean Fragility Scores with ± 1 standard deviation. Intact models are substantially more robust, while permutation-trained intact models exhibit fragility comparable to ablated models despite retaining positional embeddings.

is not perfectly preserved. This makes RPT–RPI Intact a controlled intervention that selectively disables absolute-position-based strategies without inducing the broader representational pathologies associated with PE removal.

Fragility Scores are computed identically across all regimes to ensure comparability. By contrasting the intact and ablated models with the RPT–RPI Intact model, we isolate whether robustness to spatial perturbations arises from spatial organization strategy or from the Representational Diversity introduced by the PEs. In particular, if a model trained under RPT–RPI conditions exhibits high fragility despite retaining Representational Diversity, this provides direct evidence that robustness can be explained by the differences in spatial organization strategies employed by these models. A dedicated sanity check is included to verify that RPT–RPI Intact models indeed rely on patch-content-driven cues for spatial structure, rather than implicitly recovering absolute position through degenerate shortcuts in the Appendix.

Results: We consistently find that the models that rely dominantly on patch content for spatial structure (ablated and RPT–RPI Intact models) are significantly more fragile to distributional shifts than the models that rely on an Absolute Position mode of spatial organization (Fig. 7). In particular, the RPT–RPI Intact models exhibit Fragility Scores that are substantially higher than standard intact models and nearly comparable to fully ablated models, despite retaining representational diversity. This indicates that robustness is not merely a consequence of diverse token representations, but critically depends on the presence of absolute-position-based strategies during training and inference.

Comparing intact and ablated models further clarifies the role of positional embeddings: intact models leverage PEs to construct stable spatial representations that mitigate sensitiv-

ity to random perturbations, while ablated models, lacking any absolute positional cues, show the lowest robustness. The RPT–RPI Intact regime provides a clean dissociation, showing that even when representational diversity is preserved, disruption of absolute positional mapping alone is sufficient to induce fragility.

Taken together, these results demonstrate that absolute-position-based spatial strategies, enabled by positional embeddings, are a key contributor to the stability of ViT representations under distributional shifts. Robustness cannot be explained solely by representational richness; the mode of spatial organization (absolute versus patch-relative) is a decisive factor. These findings complement our earlier analyses of representational geometry and spatial structure, linking internal organizational principles directly to functional resilience.

5. Discussion

Our results indicate that positional embeddings play a role that extends beyond injecting absolute positional information. Across models with intact positional embeddings, we consistently observe increased representational diversity in early layers, as reflected by elevated effective rank and reduced mean token-wise cosine similarity. This diversity persists weakly through depth and appears to act as a structural capacity rather than a direct determinant of performance. Notably, this capacity is necessary but not sufficient: RPT–RPI intact models retain high effective rank and low cosine similarity while exhibiting weak performance and low robustness (Appendix Fig. LALALALA). The causal role of positional embeddings is further supported by post-hoc ablation experiments, where removing positional embeddings at inference time induces an immediate collapse in effective

330 rank and increased token homogeneity, despite identical
 331 learned parameters.

332 A natural alternative explanation for these observations is
 333 that the increased effective rank and reduced cosine simi-
 334 larity associated with positional embeddings merely reflect
 335 unstructured decorrelation or noise. Several findings argue
 336 against this interpretation. Although untrained intact mod-
 337 els also exhibit high effective rank, this diversity neither
 338 collapses across depth nor is accompanied by an increase in
 339 token-wise cosine similarity. In contrast, trained intact mod-
 340 els display a coordinated pattern in which early representa-
 341 tional diversity is progressively consolidated, with effective
 342 rank collapsing and token similarity increasing across layers.
 343 This behavior is inconsistent with stochastic noise, which
 344 would be expected to persist diffusely rather than undergo
 345 selective compression. Instead, these dynamics suggest that
 346 positional embeddings introduce a high-dimensional rep-
 347 resentational capacity that training actively organizes into
 348 structured, task-aligned subspaces.

349
 350 Beyond representational geometry, positional embeddings
 351 also induce a qualitative shift in how spatial structure is
 352 formed. In the absence of positional embeddings, ViTs
 353 rely predominantly on patch content to infer relative spatial
 354 relationships, resulting in a content-based mode of spatial
 355 organization. When positional embeddings are present and
 356 combined with consistent patch ordering, models increas-
 357 ingly adopt an absolute-position-based strategy that lever-
 358 ages absolute positional information. While this aligns with
 359 common intuitions about the role of positional embeddings,
 360 our results indicate that this shift is not absolute: even intact
 361 models continue to subtly exploit patch content when form-
 362 ing spatial structure, suggesting that these strategies coexist
 363 rather than replace one another.

364
 365 Finally, this shift in spatial organization has direct implica-
 366 tions for robustness. Models that rely more heavily on
 367 absolute-position-based strategies are consistently more ro-
 368 bust to distributional shifts. In contrast, content-based spa-
 369 tial organization is particularly vulnerable to perturbations
 370 that alter local patch statistics, which can disrupt the model’s
 371 ability to infer coherent spatial relationships. This supports
 372 the interpretation that positional embeddings improve ro-
 373 bustness not simply by increasing performance, but by bi-
 374 asing ViTs toward a mode of spatial reasoning that is less
 375 sensitive to changes in patch content.

376 Taken together, these findings suggest that positional em-
 377 beddings act as a structural bias that reshapes the geometry
 378 of the representation space and alters the dominant strategy
 379 by which spatial information is encoded and used. Rather
 380 than serving as a passive positional signal, positional embed-
 381 dings influence how diversity is introduced, organized, and
 382 ultimately integrated into task-relevant computation, with
 383 measurable consequences for robustness and generalization.

Limitations and Future Directions

Despite providing a detailed mechanistic analysis, our study has several limitations. First, our experiments focus on a specific class of ViT architectures and positional embedding schemes. While we expect the qualitative distinction between absolute-position-based and patch-relative strategies to generalize, the precise dynamics may vary across architectures, embedding types, or training regimes. Extending this analysis to alternative positional encoding mechanisms, such as relative or rotary embeddings, remains an important direction for future work.

Second, our robustness evaluation centers on a particular family of distributional shifts. Although these shifts are well-motivated and commonly used, they do not exhaust the space of possible perturbations. It is possible that patch-relative strategies may confer advantages under other forms of shift not considered here.

Finally, our study is limited in its experimental scope: all analyses were conducted using relatively small Vision Transformers (12M parameters) trained on CIFAR-10. While this controlled setting enabled detailed mechanistic analysis, it raises natural questions about the generality of our findings. The magnitude of the effects we observe, such as the scale of the early-layer effective rank spike or the precise SSDC values may vary with model scale and dataset complexity. However, we hypothesize that the core directional conclusions are rooted in a causal, architectural mechanism. But we explicitly encourage future works to validate and quantify these effects in larger-scale, state-of-the-art ViT models.

6. Related Work

Positional Information in Vision Transformers

The standard Vision Transformer (ViT) breaks the permutation invariance of self-attention by adding learnable absolute positional embeddings (PEs) to patch tokens (Dosovitskiy et al., 2021), establishing the dominant paradigm for spatial encoding in vision transformers. However, it has been found that ViTs retain substantial performance even when PEs are degraded or removed (Dosovitskiy et al., 2021; Chu et al., 2023), suggesting ViTs may be able to partially recover spatial structure and implicit positional information without PEs. In fact, similar observations have been reported outside the vision domain. For example, recent work on decoder-only Transformers shows that models trained without PEs can implicitly recover positional information and that they tend to use relative positions in practice (Kazemnejad et al., 2023). While this analysis is specific to generative language models, it reinforces the broader notion that explicit PEs are not strictly required for structured positional information to emerge. This parallels earlier findings in CNNs, where

it was demonstrated that convolutional networks learn substantial positional information implicitly, for instance from architectural features like zero-padding (Islam* et al., 2020). These observations create the fundamental puzzle our work addresses: if spatial structure can emerge without explicit guidance, what functional role do PEs actually play? Prior studies on PEs in ViTs have primarily focused on architectural variants (d’Ascoli et al., 2022; Liu et al., 2021) or downstream performance comparisons [2, 3], leaving the mechanistic impact of PEs on internal representations largely unexplored.

Representational Analysis of Transformers

A separate line of work analyzes the geometry and dynamics of transformer representations using tools from representational analysis. Earlier work provided foundational comparisons between ViT and CNN representations (Raghu et al., 2021), revealing distinct spatial organization patterns. Subsequent work has examined how attention mechanisms transform representations (Kobayashi et al., 2021), and the evolution of representational rank through depth (Dong et al., 2021), and the tendency for token representations to homogenize in deep layers (Bhojanapalli et al., 2021). The residual stream framework provides the conceptual foundation for our analysis of token representations across layers (Elhage et al., 2021). However, despite these insights, these representational analyses have not specifically targeted the causal effect of positional embeddings on this geometry, nor have they connected these internal dynamics to external robustness properties.

Robustness of Visual Models

Vision Transformers exhibit distinct robustness profiles compared to convolutional networks. Prior works have systematically compared ViT and CNN robustness, finding transformers exhibit greater resilience to spatial perturbations but increased sensitivity to certain texture changes (Bhojanapalli et al., 2021). Subsequent work further establishes that ViTs demonstrate favorable out-of-distribution generalization properties (Paul & Chen, 2022). These observations connect to the broader literature on shape versus texture bias in visual recognition, where it has been shown that models with stronger shape bias tend to exhibit better generalization (Geirhos et al., 2019). While robustness differences between architectural families have been documented, the link between a model’s specific spatial reasoning strategy, such as relying on absolute position versus inferring relations from content, and its robustness to distribution shifts has not been mechanistically established.

Our Contribution

We bridge these disconnected research threads to solve the positional embedding puzzle. Unlike performance-focused ablation studies (Dosovitskiy et al., 2021; Chu et al., 2023),

we perform a causal, representational analysis to show how PEs work internally. We demonstrate they (1) induce early-layer representational diversity through a high-rank injection at layer 0, (2) shift the model’s spatial organization strategy from content-relative to position-absolute reasoning, and (3) that this strategic shift—rather than representational diversity alone—confers robustness to texture-based distribution shifts. We introduce the Spatial Similarity Distance Correlation (SSDC) metric and employ controlled interventions like Random Permutation Training to isolate these mechanisms, providing the a unified and mechanistic account of why PEs remain crucial beyond their basic function of breaking permutation invariance.

7. Conclusion

In this work, we investigated how positional embeddings shape spatial organization and representation geometry in Vision Transformers. We show that even in the absence of positional embeddings, ViTs retain non-trivial spatial structure through a patch-relative, content-based mode of organization. However, this structure is fragile and corresponds to limited representational consolidation. When positional embeddings are present, they introduce substantial early-layer representational diversity and induce a qualitatively different pattern of representation dynamics, characterized by coordinated rank collapse and increased token similarity across depth.

These findings indicate that positional embeddings act as a structural bias that alters both the geometry of the latent space and the dominant strategy by which spatial information is encoded. By pushing ViTs toward an absolute-position mode of spatial organization, positional embeddings promote more stable and robust representations under distributional shift, while still allowing patch content to play a secondary role. More broadly, our results suggest that spatial reasoning in ViTs emerges from the interaction between inductive bias, training dynamics, and representational geometry, rather than from positional encoding alone. Understanding and controlling these interactions may be critical for designing transformer-based vision models that generalize reliably beyond their training distributions.

References

- Bhojanapalli, S., Chakrabarti, A., Glasner, D., Li, D., Unterthiner, T., and Veit, A. Understanding robustness of transformers for image classification. pp. 10211–10221, 10 2021. doi: 10.1109/ICCV48922.2021.01007.
- Chu, X., Tian, Z., Zhang, B., Wang, X., and Shen, C. Conditional positional encodings for vision transformers. In *The Eleventh International Conference on Learning Representations*, 2023. URL <https://openreview.net/>

- 440 forum?id=3KWnuT-R1bh.
- 441
- 442 Dong, Y., Cordonnier, J.-B., and Loukas, A. Attention
443 is not all you need: pure attention loses rank doubly
444 exponentially with depth. In Meila, M. and Zhang, T.
445 (eds.), *Proceedings of the 38th International Conference
446 on Machine Learning*, volume 139 of *Proceedings of
447 Machine Learning Research*, pp. 2793–2803. PMLR, 18–
448 24 Jul 2021. URL <https://proceedings.mlr.press/v139/dong21a.html>.
- 449
- 450
- 451 Dosovitskiy, A., Beyer, L., Kolesnikov, A., Weissenborn,
452 D., Zhai, X., Unterthiner, T., Dehghani, M., Minderer,
453 M., Heigold, G., Gelly, S., Uszkoreit, J., and Houlsby,
454 N. An image is worth 16x16 words: Transformers for
455 image recognition at scale. In *International Conference
456 on Learning Representations*, 2021. URL <https://openreview.net/forum?id=YicbFdNTTy>.
- 457
- 458 d’Ascoli, S., Touvron, H., Leavitt, M. L., Morcos, A. S.,
459 Biroli, G., and Sagun, L. Convit: improving vision
460 transformers with soft convolutional inductive biases*.
461 *Journal of Statistical Mechanics: Theory and Experiment*,
462 2022(11):114005, nov 2022. doi: 10.1088/1742-5468/ac9830. URL <https://doi.org/10.1088/1742-5468/ac9830>.
- 463
- 464
- 465
- 466 Elhage, N., Nanda, N., Olsson, C., Henighan, T., Joseph,
467 N., Mann, B., Askell, A., Bai, Y., Chen, A., Conerly,
468 T., DasSarma, N., Drain, D., Ganguli, D., Hatfield-
469 Dodds, Z., Hernandez, D., Jones, A., Kernion, J., Lovitt,
470 L., Ndousse, K., Amodei, D., Brown, T., Clark, J.,
471 Kaplan, J., McCandlish, S., and Olah, C. A mathematical
472 framework for transformer circuits. *Transformer Circuits Thread*, 2021. <https://transformercircuits.pub/2021/framework/index.html>.
- 473
- 474
- 475
- 476 Geirhos, R., Rubisch, P., Michaelis, C., Bethge, M., Wich-
477 mann, F. A., and Brendel, W. Imagenet-trained CNNs
478 are biased towards texture; increasing shape bias im-
479 proves accuracy and robustness. In *International Confer-
480 ence on Learning Representations*, 2019. URL <https://openreview.net/forum?id=Bygh9j09KX>.
- 481
- 482 Islam*, M. A., Jia*, S., and Bruce, N. D. B. How much
483 position information do convolutional neural networks en-
484 code? In *International Conference on Learning Repres-
485 entations*, 2020. URL <https://openreview.net/forum?id=rJeB36NKvB>.
- 486
- 487
- 488 Kazemnejad, A., Padhi, I., Natesan, K., Das, P., and
489 Reddy, S. The impact of positional encoding on
490 length generalization in transformers. In *Thirty-seventh
491 Conference on Neural Information Processing Systems*,
492 2023. URL <https://openreview.net/forum?id=Drrl2gcjzl>.
- 493
- 494
- 495 Kobayashi, G., Kurabayashi, T., Yokoi, S., and Inui,
496 K. Incorporating Residual and Normalization Lay-
497 ers into Analysis of Masked Language Models. In Moens,
498 M.-F., Huang, X., Specia, L., and Yih, S. W.-t. (eds.),
499 *Proceedings of the 2021 Conference on Empirical
500 Methods in Natural Language Processing*, pp. 4547–4568. Association for Computational Linguistics,
501 November 2021. doi: 10.18653/v1/2021.emnlp-main.
502 373. URL <https://aclanthology.org/2021.emnlp-main.373>.
- 503
- 504 Liu, Z., Lin, Y., Cao, Y., Hu, H., Wei, Y., Zhang, Z., Lin,
505 S., and Guo, B. Swin Transformer: Hierarchical Vision
506 Transformer using Shifted Windows . In *2021 IEEE/CVF
507 International Conference on Computer Vision (ICCV)*,
508 pp. 9992–10002. IEEE Computer Society, October
509 2021. doi: 10.1109/ICCV48922.2021.00986. URL
510 <https://doi.ieee.org/10.1109/ICCV48922.2021.00986>.
- 511
- 512 Paul, S. and Chen, P.-Y. Vision transformers are robust learn-
513 ers. *Proceedings of the AAAI Conference on Artificial
514 Intelligence*, 36(2):2071–2081, Jun. 2022. doi: 10.1609/
515 aaai.v36i2.20103. URL <https://ojs.aaai.org/index.php/AAAI/article/view/20103>.
- 516
- 517 Raghu, M., Unterthiner, T., Kornblith, S., Zhang, C., and
518 Dosovitskiy, A. Do vision transformers see like convolu-
519 tional neural networks? In Beygelzimer, A., Dauphin, Y.,
520 Liang, P., and Vaughan, J. W. (eds.), *Advances in Neural
521 Information Processing Systems*, 2021. URL <https://openreview.net/forum?id=R-616EWWKF5>.

A. Experimental Setup and Hyperparameters

Table 1. Model architecture and training hyperparameters used in all experiments.

Parameter	Value
<i>Input & Tokenization</i>	
Input resolution	32×32
Patch size	4×4
Number of patches	64
Input channels (C)	3
<i>ViT Architecture</i>	
Embedding dimension (D)	320
Number of encoder layers	10
Number of attention heads	8
Key/query dimension (d_k)	40
Dropout (embedding)	0.1
Dropout (attention)	0.1
Dropout (MLP)	0.1
Stochastic depth rate	0.1
<i>Training Hyperparameters</i>	
Batch size	128
Optimizer	Adam
Learning rate	1×10^{-3}
Weight decay	5×10^{-4}
Adam β_1	0.9
Adam β_2	0.999
Training epochs	50

B. Metric Definitions and Implementation Details

B.1. Spatial Similarity Distance Correlation (SSDC)

Let T denote the number of patch tokens (excluding the CLS token), arranged on a $\sqrt{T} \times \sqrt{T}$ image grid. For a given layer, let $S \in \mathbb{R}^{T \times T}$ be the pairwise cosine similarity matrix between token representations. We associate each token i with spatial coordinates $\mathbf{p}_i \in \mathbb{Z}^2$ corresponding to its location on the image grid, and define the spatial distance matrix $D \in \mathbb{R}^{T \times T}$ by

$$D_{ij} = \|\mathbf{p}_i - \mathbf{p}_j\|_1,$$

where $\|\cdot\|_1$ denotes Manhattan distance.

SSDC is defined as the Spearman rank correlation between representational similarity and negative spatial distance over all unordered token pairs:

$$\text{SSDC} = \rho_{\text{Spearman}}(\{S_{ij}\}_{i < j}, \{-D_{ij}\}_{i < j}).$$

Higher SSDC values indicate that spatially proximal tokens tend to have more similar representations, reflecting stronger relative positional structure in the residual stream. We use Spearman correlation to remain agnostic to the exact functional relationship between spatial distance and representational similarity.

Effective Rank

Given a matrix $X \in \mathbb{R}^{n \times d}$ (e.g., a collection of token representations), let $\sigma_1, \dots, \sigma_r$ denote its singular values, where $r = \text{rank}(X)$. We define the effective rank of X using the participation ratio as

$$\text{erank}(X) = \frac{\left(\sum_{i=1}^r \sigma_i^2\right)^2}{\sum_{i=1}^r \sigma_i^4}.$$

550 This quantity measures how evenly variance is distributed across singular directions: it attains its maximum value of r when
 551 all singular values are equal, and decreases as the representation collapses onto fewer dominant directions.
 552

553 B.2. Mean Cosine Similarity

554 Let $R \in \mathbb{R}^{B \times T \times D}$ denote the token representations at a given layer, excluding the [CLS] token, where B is the batch
 555 size, T the number of tokens, and D the hidden dimension. For each sample in the batch, we compute the pairwise cosine
 556 similarity between all token representations to obtain a token cosine similarity matrix $S \in \mathbb{R}^{T \times T}$, where
 557

$$S_{ij} = \frac{r_i^\top r_j}{\|r_i\|_2 \|r_j\|_2}.$$

561 The similarity matrices are symmetric by construction and have unit diagonal. We average S across the batch dimension to
 562 obtain a layer-wise summary of inter-token relationships. Mean Cosine Similarity (MCS) is defined as the mean of all entries
 563 of this averaged similarity matrix. Because the diagonal entries are identically equal to 1 across all models and conditions,
 564 including them does not affect comparative analysis. Higher MCS values indicate greater representational homogeneity
 565 among tokens.
 566

567 B.3. Fragility Score

568 To quantify sensitivity to distributional shifts, we compute the Fragility Score (FS), defined as the relative drop in top-1
 569 accuracy under a given shift:
 570

$$\text{FS} = 1 - \frac{A_{\text{shift}}}{A_{\text{normal}}},$$

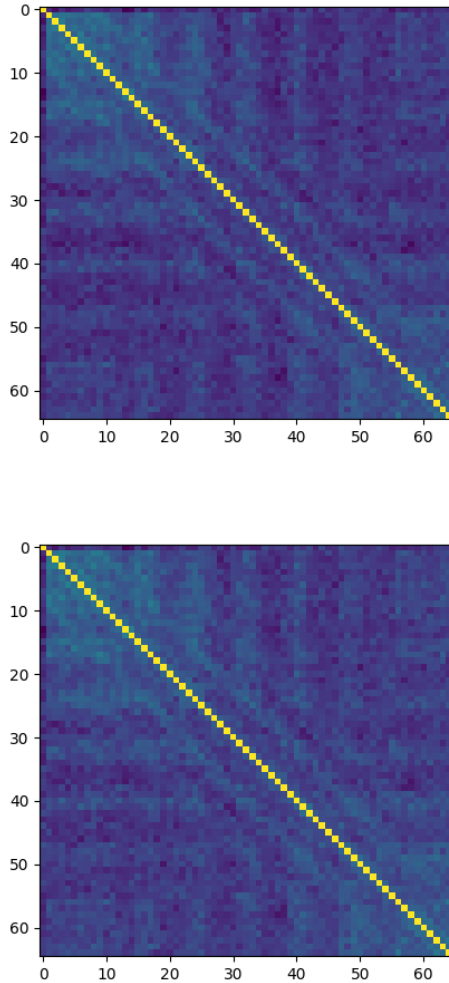
571 where A_{normal} and A_{shift} denote top-1 accuracy on the unshifted and shifted datasets, respectively. Higher values correspond
 572 to greater performance degradation. Unless otherwise stated, accuracies are averaged across random seeds prior to computing
 573 FS.
 574

575 B.4. Metric Summary

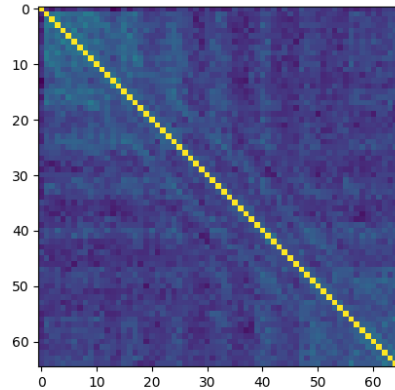
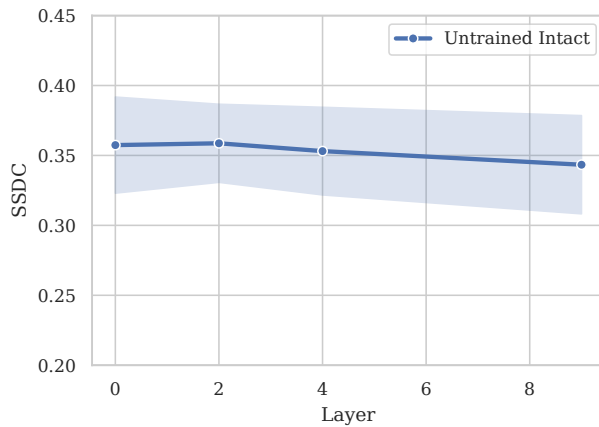
576 For clarity, we briefly summarize the metrics used throughout this work and the phenomena they are intended to capture.
 577

- 578 • **Mean Cosine Similarity (MCS)** measures average pairwise similarity between token representations and serves as a proxy for inter-token homogeneity or redundancy.
- 579 • **Effective Rank** quantifies representational diversity by measuring how evenly variance is distributed across singular directions of the token representation matrix.
- 580 • **Spatial Similarity Distance Correlation (SSDC)** captures the degree to which representational similarity aligns with spatial proximity, serving as a proxy for relative positional structure in the residual stream.
- 581 • **Fragility Score (FS)** measures sensitivity to distributional shifts by quantifying relative performance degradation under dataset perturbations.

582 Together, these metrics allow us to disentangle representational diversity, spatial organization strategy, and robustness, and to analyze how positional embeddings causally affect each of these factors.
 583

605 C. Additional Analyses
606607 C.1. Spatial Structure in Untrained Ablated Models
608609
610
611
612
613
614
615
616
617
618
619
620
621
622
623
624
625
626
627
628
629
630
631
632
633
634
635
636
637
638
639
640
641
642643 Figure 9. Batch-averaged token cosine similarity heatmaps for an untrained ablated (NoPE) model at layers 0 (top) and 2 (bottom). A
644 diagonal spatial structure is present at initialization, but remains unchanged across layers, indicating static, architecture-induced spatial
645 organization rather than learned positional structure.
646647 To complement the quantitative SSDC results reported in the main text, we visualize token cosine similarity heatmaps
648 for untrained ablated (NoPE) models. Figure 9 shows batch-averaged token cosine similarity matrices at layers 0 and 2,
649 excluding the [CLS] token.650 Despite the absence of training, a clear diagonal structure is already present at initialization, indicating that a weak form of
651 spatial organization is implicitly induced by the model architecture and the image patchification process. However, this
652 structure does not sharpen, diffuse, or qualitatively change across early layers, remaining essentially invariant through depth.
653 This behavior contrasts with trained models, where spatial structure evolves with depth and reflects learned spatial reasoning
654 strategies.
655656 These visualizations support the interpretation that spatial structure observed in untrained ablated models is not emergent,
657 but rather a static byproduct of architectural and data-induced biases.
658

660
661
662
663
664
665
666
667
668
669
670
671
672
673
674



(a) **SSDC Across Depth for an Untrained Intact Model.** SSDC remains consistently low and invariant across depth ($n = 3$ seeds), indicating an absence of coherent spatial structure despite the presence of positional embeddings.

(b) **Representative Token Cosine Similarity Matrix from an Untrained Intact Model.** The weak diagonal pattern and low overall inter-token similarity reflect disrupted spatial correlations induced by untrained positional embeddings.

Figure 10. (

Spatial Structure in Untrained Intact Models. Untrained positional embeddings suppress spatial structure by injecting unstructured positional perturbations, resulting in low SSDC and weak token-to-token correlations across depth.)

C.2. Absence of Spatial Structure in Untrained Intact Models

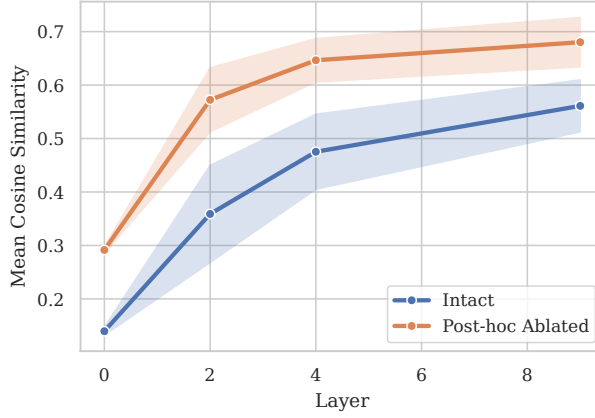
We observe that SSDC in the untrained intact model remains consistently low and invariant across depth. This behavior contrasts sharply with untrained ablated models and indicates an absence of coherent spatial structure. We attribute this effect to the presence of untrained positional embeddings, which introduce unstructured positional perturbations that disrupt the weak spatial correlations otherwise present in ViTs without positional encodings (Sections 4.1 and C.1).

This interpretation is supported by the representative Token Cosine Similarity Matrix in Figure 10, which exhibits a substantially weaker diagonal structure and lower overall inter-token similarity compared to the untrained ablated model (Figure 9). Together, these observations indicate that the representational diversity observed in untrained intact models does not reflect meaningful spatial organization, but rather the injection of positional noise.

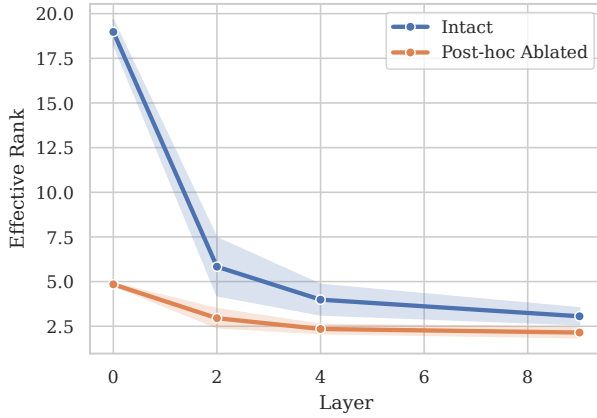
In contrast, the trained intact model exhibits markedly different behavior: SSDC begins at a higher value and increases sharply from layer 0 to layer 2 (Figure 2). When considered alongside the depth-wise evolution of representational diversity, this divergence highlights a key distinction between noise-induced diversity in untrained intact models and the emergence of functionally meaningful spatial structure during early stages of training.

694
695
696
697
698
699
700
701
702
703
704
705
706
707
708
709
710
711
712
713
714

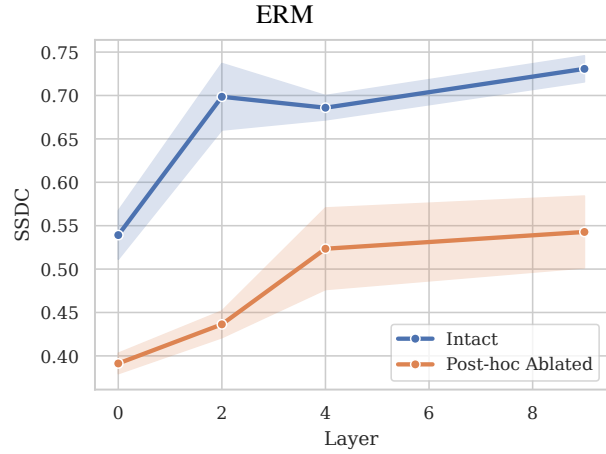
C.3. Effects of Post-hoc Ablation of Positional Embeddings



(a) **Mean Cosine Similarity Across Depth With and Without Positional Embeddings.** Removing positional embeddings from a trained Intact model increases similarity among token representations in early layers, reflecting a collapse of representational diversity. Intact models maintain lower early-layer similarity, highlighting the role of positional embeddings in structuring diverse representations.



(b) **Effective Rank Across Depth With and Without Positional Embeddings.** Post-hoc ablation of positional embeddings substantially reduces effective rank, particularly in early layers, confirming that positional information supports the spread and dimensionality of learned representations. Intact models maintain higher rank across layers.



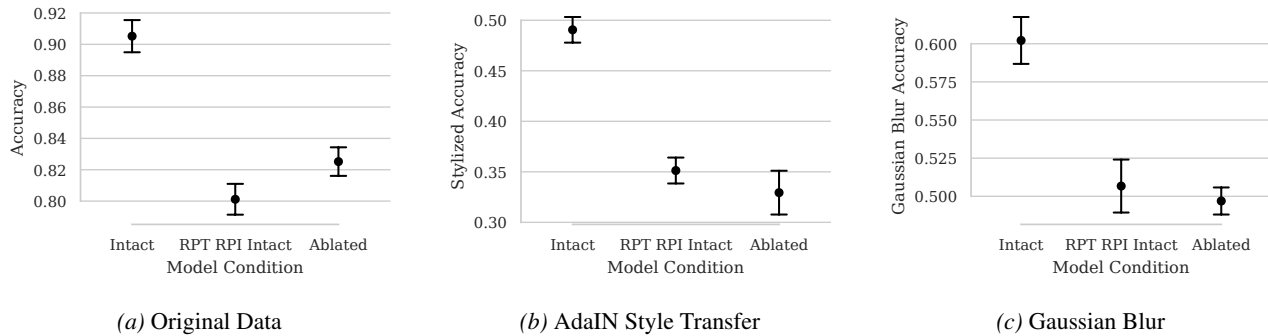
(c) **SSDC Across Depth With and Without Positional Embeddings.** Removing positional embeddings lowers initial SSDC and delays the characteristic peak from layer 2 to around layer 4, which is also weaker in magnitude. This indicates that positional embeddings accelerate the formation of spatial structure in early layers and contribute to its overall magnitude.

Figure 11. Effects of Post-hoc Positional Embedding Removal. Removing positional embeddings from a trained Intact model causes both representational diversity and SSDC to collapse.

Upon post-hoc removal of positional embeddings from an Intact model, representational diversity collapses immediately, as expected. More interestingly, SSDC also decreases: the initial value at layer 0 is lower, and the characteristic peak observed in intact models shifts to later layers (around layer 4) and is weaker in magnitude (Figure 11). This indicates that positional embeddings not only contribute to the overall level of spatial structure but also accelerate its early-layer development. These results confirm that the learned representations in Intact models rely on positional information to establish and maintain both representational diversity and spatial organization, rather than solely on patch-content correlations.

770 771 772 773 774 775 776 777 C.4. Model Performance Across Distributional Shifts

778 We evaluate the absolute performance of our models under three conditions: the original (in-distribution) data, AdaIN
779 style transfer, and Gaussian blur. Figures 12a, 12b, and 12c summarize the results. Across all settings, the Intact model
780 consistently outperforms both the Ablated and RPT-RPI Intact models, which exhibit similar and substantially lower
781 accuracies. This pattern highlights that removing or perturbing positional embeddings diminishes functional performance,
782 while the Intact model retains robustness even under distributional shifts.

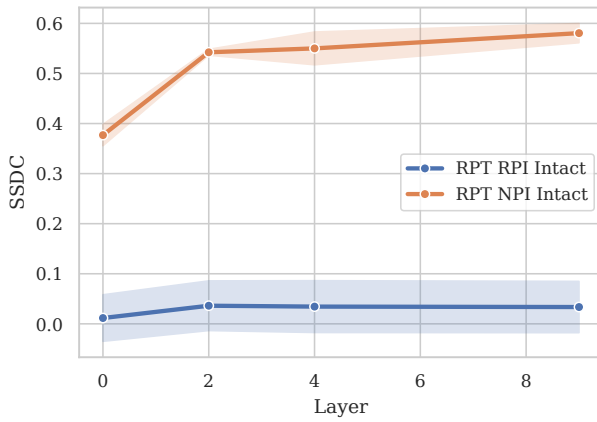


783 **Figure 12. Absolute Model Accuracies Across Distributional Shifts.** Intact models maintain substantially higher performance across all
784 shifts, whereas Ablated and RPT-RPI Intact models exhibit similar, lower accuracies. This trend underscores the functional importance of
785 intact positional embeddings.

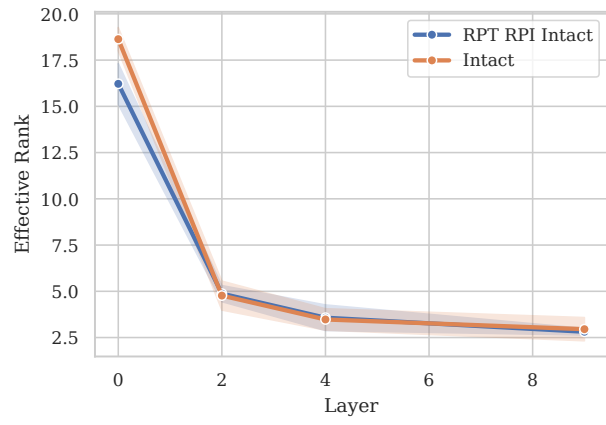
786 D. Sanity Checks

787 D.1. Patch Content Reliance in RPT RPI Intact Models

788 Together, these results confirm that RPT–RPI Intact models preserve substantial representational diversity while relying on
789 patch-content alignment for spatial organization. The near-zero SSDC under permutation, coupled with the recovery of
790 healthy SSDC dynamics when permutations are removed at inference (RPT–NPI Intact), demonstrates that spatial structure
791 is present but expressed through content-dependent rather than absolute positional cues. The close correspondence in
792 Effective Rank further verifies that this behavior is not driven by representational collapse. These observations serve as
793 a sanity check that RPT–RPI Intact models behave consistently with their intended design and that our metrics reliably
794 distinguish spatial structure from representational diversity.



(a) **Spatial Structure in RPT–RPI Intact Models.** SSDC in RPT–RPI Intact models remains near zero across depth, indicating the absence of stable spatial structure under random patch permutations. When the permutation is removed at inference (RPT–NPI Intact), SSDC exhibits non-zero values and characteristic early-layer growth between layers 0 and 2, consistent with healthy trained models. This behavior confirms that spatial structure in RPT–RPI Intact models is primarily dependent on patch-content alignment rather than absolute position. These findings are consistent across runs ($n=3$ seeds).



(b) **Representational Diversity in RPT–RPI Intact Models.** Effective Rank across layers for Intact and RPT–RPI Intact models largely overlaps, with only a slight reduction in the first layer for RPT–RPI Intact models. This indicates that representational diversity is largely preserved under random patch permutations, despite the absence of stable spatial structure.

Figure 13. Spatial Structure and Representational Diversity in RPT–RPI Intact Models. This figure compares spatial structure and representational diversity in RPT–RPI Intact models and their non-permuted inference counterpart (RPT–NPI Intact), where patch permutations are removed at inference. SSDC remains near zero under random patch permutations but recovers healthy early-layer growth when permutations are removed, indicating content-dependent spatial structure. Effective Rank closely matches that of fully Intact models across layers, with only a slight reduction in the first layer, confirming that representational diversity is largely preserved. Together, these results validate that RPT–RPI Intact models maintain diverse representations while expressing spatial structure primarily through patch-content alignment.